Scientific Publications

World Journal of Cancer and Oncology Research, 2026, 5, 6439
www.scipublications.com/journal/wjcor
DOI: 10.31586/wjcor.2026.6439

Seminar in Writing

Magnetic-flux-density based rational designing of 100kHz electromagnetic-field radiator for nano-thermal ablation therapy

Tomio Morino [1,*], Noriyasu Kawai [2], Takahiro Yasui [3]

[1] Former visiting professor, Department of Nephro-urology, Nagoya City University Graduate School of Medical Sciences, 1 Kawasumi, Mizuho-cho, Mizuho-ku, Nagoya 467-8601, Japan

[2] Department of Urology, Nagoya City University Midori Municipal Hospital, 1-77 Shiomigaoka, Midori-ku, Nagoya 458−0037, Japan

[3] Department of Nephro-urology, Nagoya City University Graduate School of Medical Sciences, 1 Kawasumi, Mizuho-cho, Mizuho-ku, Nagoya 467-8601, Japan

* Correspondence: Tomio Morino (moritomi2025@gmail.com)

Abstract: We have reported novel solid-cancer treatment modality of nano-thermal ablation therapy using two medical devices of 100kHz electromagnetic field radiator and heat-generating nanoparticles of MCL particle [1]. External 100kHz electromagnetic field radiation induced heat generation of MCL particle in tumor tissue and caused tumor specific cytotoxicity and blood vessel disruption [1]. MCL particle was designed to be about 100nm diameter and to move within tumor tissue by composing heat-generating magnetite (Fe_3O_4) with neutral and cationic lipids [1]. However, concerning 100kHz radiator, rational concept of its performance and specification was not fully discussed. Purpose of this seminar is to describe significance of 100kHz magnetic flux density for rational designing, specification and usage of the radiator, referring to our unpublished data during 2004~2025. At first, our calibration method of 100kHz magnetic flux density was shown, and then its application to density distribution analysis of our radiators HTS-5010H and Hi-Heater 5010 was described. And, based on density distribution profile of Hi-Heater 5010 radiator, effective density at tumor locus in the standard treatment condition of the therapy was confirmed 15mT. Based on the recorded data of clinical research using HTS-5010H radiator, safety radiation condition toward groin, breast, thigh, neck, chest and arm were shown with density distribution in patient bodies. With all respect, quoting MFH®300F (100kHz) radiator [2], availability of three types radiators for various target cancers was discussed on the basis of effective tumor density and mitigation of normal tissue heating. According to Design Control Guidance of medical device [3], design process of the radiator was exemplified by drafted documents of design input and output.

Keywords: Solid Cancer Therapy; Nano-Thermal Ablation Therapy; Magnetic Flux Density; Heat Generating Nanoparticle; MCL Particle; Hysteresis Loss; Eddy Current Loss; Design Control; Design History File

How to cite this paper:
Morino, T.; Kawai, N.; Yasui, T. (2026). Magnetic-flux-density based rational designing of 100kHz electromagnetic-field radiator for nano-thermal ablation therapy. *World Journal of Cancer and Oncology Research, 5*(1), 1-12. DOI: 10.31586/wjcor.2026.6439

Academic Editor:
Mohamed Kotb El-Sayed

Received: May 21, 2026
Revised: June 22, 2026
Accepted: June 27, 2026
Published: June 29, 2026

1. Historical background of 100kHz radiators for cancer therapy

Basic deliberation of electromagnetic field radiator used for cancer therapy using heat generating materials had been described by Gilchrist R. et.al in 1957 [4]. The first proposer of this treatment modality had indicated two formulas of heat generation on efficacy and safety-concerns. One on efficacy was heating from materials located in tumor tissue, based on hysteresis loss theory [4] p.600, and the other on safety-concerns was heating from normal biological tissue, based on Eddy current loss theory [4] p599. These two formulas

were conceptually identical to currently used following formulas, which were the theoretical background of this seminar.

Formula 1 on efficacy; heating from material

$$W = \eta \cdot f \cdot B_m^{1.6} V \quad (1)$$

W: hysteresis loss (watt = joule (J)/sec)
η : hysteresis coefficient
f : frequency of magnetic cycles (Hz)
B_m: magnetic flux density at maximum (T)
(the exponent 1.6 is typical for silicon steel)
V : volume of the material (m^3)

Formula 2 on safety-concerns; heating from normal biological tissue

$$P = \sigma(\pi f r B)^2 \quad (2)$$

P : power absorbed per unit volume (W/m^3 = joule (J)/sec, m^3)
σ : electrical conductivity of tissue (S/m)
f : magnetic field frequency (Hz)
B : magnetic flux density (T)
r : radius of the induced current loop (body region) (m)

Two formulas indicated the first subject to optimize electromagnetic field frequency (Hz), since material heating increased proportionally with frequency, whereas normal biological tissue heating increased with frequency squared. In accordance with this behavior, relatively low frequency between 55~450kHz has been applied to animal tumor models by several groups [5-8] including Japanese one [8]. And, due to tumor regression efficacy and radiation safety in whole animal body, a frequency of human-unfamiliar 100kHz was selected for clinical study by Johanssen M. et al. [9], Maier-Hauff K. et al. [10] and Japanese group [11], [12] p.1721.

Two formulas indicated the second subject to control magnetic flux density (T), since both heating on efficacy and safety-concerns were commonly determined by the density. However, cancer therapy using heat generating material had sought tumor temperature rise (℃), heating value (J) from material and its determinant of magnetic flux density (T) were concerned little or overlooked.

In 2020 we have discussed irrationality of tumor-temperature index in our therapy using MCL particle and showed alternative heat-dose index represented with heating value of joule (J) [13,14]. Thus, in our therapy, measurement of magnetic flux density has become critical and urgent subject to control the material heating (**Formula 1**). And fortunately, this motivation reminded us methodology to mitigate normal tissue heating on the basis of the density distribution in human body (**Formula 2**).

This seminar summarized unpublished data of the density-related study during 2004~ 2025 and showed rational concept of 100kHz electromagnetic field radiator used in nano-thermal ablation therapy [1]. The seminar tended to discuss developmental subjects rather than to peruse scientific interests. Data were shown in comprehensive order, not always in chronological order of our research.

2. Concept of radiator construction for clinical use

In 2004, a group to develop the therapy using MCL particle [8] was organized in Japan. In the same year, Gneveckow U. et al. reported an epoch-making MFH®300F radiator at 100kHz, which had gap zone between two 20cm Φ coils for laid human body in order to treat wide range cancers including deep-seated one [2]. Then, we decided to

focus on another type of 100kHz radiator, which have one 7cm Φ coil to radiate limited skin surface area in order to treat skin-closed cancers. For proof of concept, we considered skin-closed cancer was practical target, because of certainty of external MCL particle injection.

According to Design Control Guidance [3], we have drafted "design input" as; "the radiator shall irradiate target tumor with MCL particles under limited irradiation condition in order to mitigate exposure of normal tissue and temperature rise at irradiated healthy skin".

2.1. Designing of HTS-5010H and Hi-Heater 5010 radiators

HTS-5010H radiator (**Figure 1a**) was designed to have movable radiation part (**Figure 1b**), which built in radiation unit composed of one coil (7cm inner Φ, 11 turns) and cyrindorical ferrite-core (relative trans-magentic value of 3000~4000, near-lossless Monzon FC, TDK, Tokyo) (**Figure 1c**).

On the other hand, Hi-Heater 5010 radiator (**Figure 2a**) was designed to treat rather distal cancers from skin surface. Radiation unit of hat-shaped coil and protrusive ferrite-core (**Figure 2b, 2c**) was built in main body to radiate upper direction (**Figure 2a**).

Both radiatiors were composed of power supply unit, impedance matching unit, radiation coil unit and coolant circulation unit. Output power was changeable under maximum 10kW and 11kW respectively. Cooling jacket was located between coil and ferrite core, and radiation unit was sealed with insulator cover board. Redundant space from coil edge to outside surface of cover board (hereafter, radiation surface) were about 10mm.

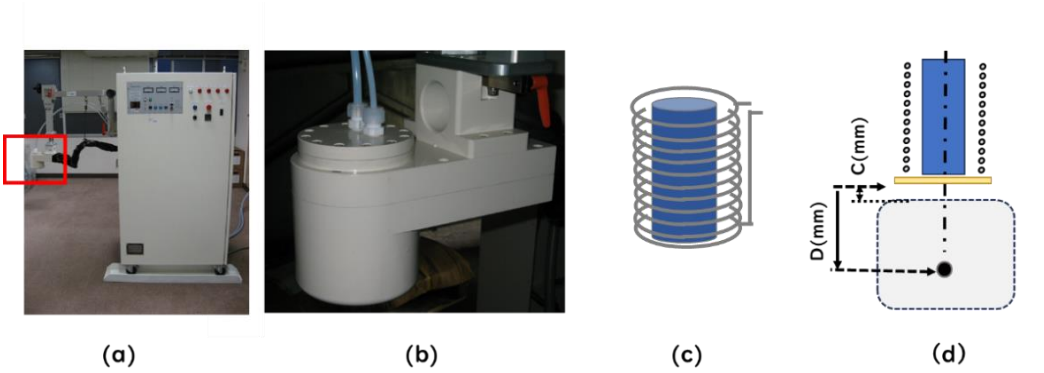

Figure 1. HTS-5010H radiator with movable radiation part (**a**) Overviewing. Radiation part was marked with red square; (**b**) Enlarged radiation part; (**c**) Radiation unit built in radiation part. Ferrite core (blue) was inserted in a coil (gray). Cooling jacket was not shown in this figure.; (**d**) Scheme in use shown with radiation coil, ferrite core, cover board (yellow), human body (light gray) and target tumor (black circle).

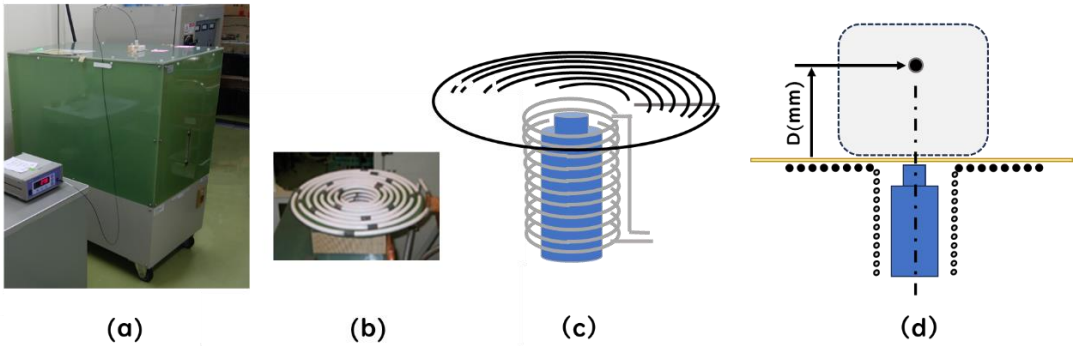

Figure 2. Hi-Heater 5010 radiator with another coil unit for distal cancer treatment (**a**) Overviewing; (**b**) Trial product of hat-shaped coil; (**c**) Radiation unit composed of hat-shaped coil (black and gray) and protrusive ferrite core (blue); (**d**) Scheme in use.

2.2. Clinical operation of HTS-5010H and Hi-Heater 5010 radiators

Before radiation, coil-center axis of coil unit was adjusted toward tumor center (**Figure 1d**, **2d**). Distance from radiation surface to tumor center was defined D (mm) and clearance from radiation surface to patient skin surface was defined C (mm) (**Figure 1d**, **2d**). Magnetic flux density at tumor locus was specified with output power (kW), distance D (mm) and clearance C (mm) as described later.

3. Ability to form 100kHz magnetic flux density

In 2005, we have fixed composition of radiation unit of HTS-5010H radiator and planned to test its ability of magnetic flux density formation. However, at that time, gauss meter of 100kHz frequency was not commercially available, and we applied gauss-meter of 50~60Hz frequency, which was used for environment assessment of electric transmission line (ELT-400, Narda safety test solution GmbH, 3cmΦ sensor). After this trial use, we decided to develop calibration method of 100kHz magnetic flux density by ourselves. This study has been started in 2005 and refined after reporting of heat-dose index in 2020 [13,14].

3.1. Public and professional exposure limit of HTS-5010H radiator

Magnetic flux density at 100kHz formed at maximum output power 10kW was measured by the gauss meter of 50~60Hz in stepwise from distal position toward radiation part. Exposure limits for public (6.25μT) and professional (18μT) were shown, and density enrichment in radiation direction was observed (**Figure 3**). However, getting closer to radiation part, the gauss meter began to heat and was finally destroyed around 1mT. Since other providers' meters had similar usage and specification, we decided to develop calibration method for high density range by ourselves.

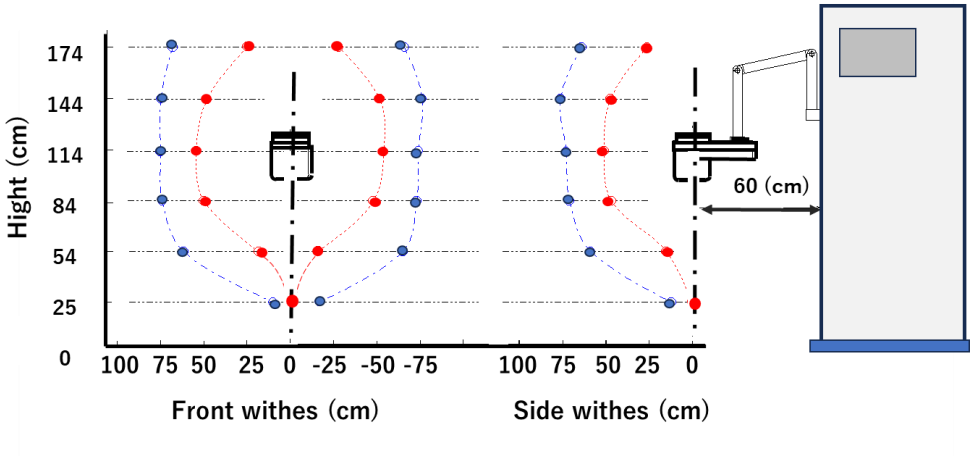

Figure 3. Public and professional exposure limits of HTS-5010H radiator, according to ICNIRP guide line, public (6.25μT, blue line) and professional (18μT, red line) exposure limits of 100kHz magnetic flux density were tested under output power 10kW.

3.2. Calibration of 100kHz magnetic flux density over 1mT

It was well known that magnetic flux density in vacant solenoid coil (**Figure 4a**) could be tuned by electric current as shown following formula; Magnetic flux density (T) = absolute permeability in vacuum X relative magnetic permeability in air X electric current (A) X coil turn number / coil length. On the other hand, we have showed correlation of magnetite heating to magnetic field strength [15] p.8. Then, we tried to calibrate the density by means of temperature rise of magnetite-containing phantom block.

Phantom block was made from refined magnetite granule and liquified polyethylene resin with variation of magnetite contents. The mixture of 2ml was solidified in 13mm cubic block, and 1mmΦ hole was drilled for temperature probe insertion (**Figure 4b**). Phantoms with temperature probe (Thermometer FX-9020, Anritsu Meter Co. Tokyo) was set in solenoid coil center and temperature rise during 5min was tested under density-tuned condition. As a result, correlation of the density to temperature rise was shown (**Figure 5**). In density less than 30mT, appropriate phantom block was selected due to calibration range. In density over 30mT, duration of temperature rise was shortened to 2.5 min (**Figure 5**).

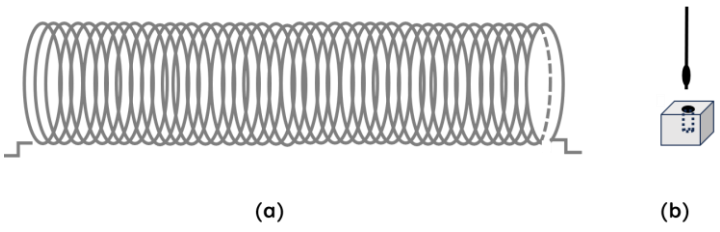

Figure 4. Tools for calibration of 100kHz magnetic flux density (**a**) Vacant solenoid coil at 100kHz; (**b**) Optic temperature probe (upper) was inserted in 1mm hole of magnetite containing phantom block (lower).

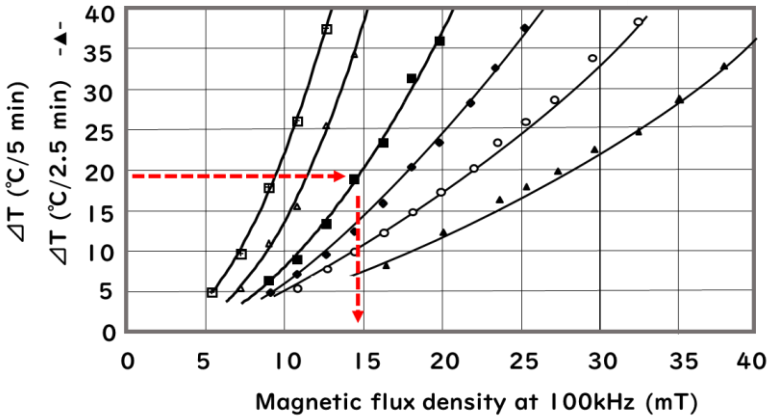

Figure 5. Calibration of 100kHz magnetic flux density using magnetite containing phantom blocks, temperature rise of phantom blocks during 5 min was tested under density-tuned conditions with variation of magnetite contents; 60 mg (⊡), 40mg (△), 20mg (■), 15mg (◈) and 10mg (○) magnetite. Exceptionally, for calibration over 30mT, temperature rise during 2.5min was tested with 15mg magnetite block (▲). Red dotted arrows showed calibration example as described later.

3.3. Analysis of the density distribution of HTS-5010H and Hi-Heater 5010 radiators

In order to show ability of magnetic flux density formation, temperature rise of phantom block was tested at distance D (mm) on coil center axis (**Figure 6a, 6b**). For example, in HTS-5010H radiator, phantom block with 20mg magnetite, located at D=15mm and radiated at output power 4.9kW showed temperature rise of 19.2℃. The density of this radiation condition was calibrated 14.6mT as shown in **Figure 5**.

In similar fashion, densities on coil center axis of two radiators were tested under annotated output power (**Figure 6c, 6d**). Density distribution profile of HTS-5010H radiator was represented with exponential function of density (y axis) and distance from radiation surface (x axis) as; $y = 28.6\ e^{-0.044x}$ at 4.9kW and $y = 35.8\ e^{-0.045x}$ at 8.8kW. On the other hand, Hi-Heater 5010 radiator showed almost-linear density declining and achieved high density at distal position from radiation surface.

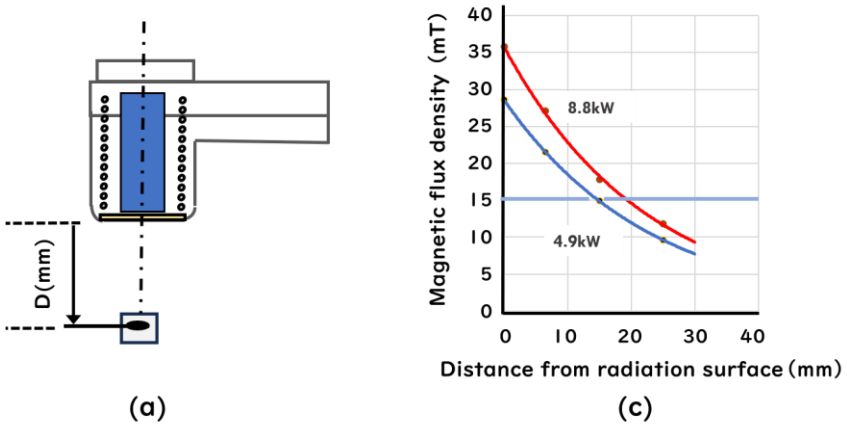

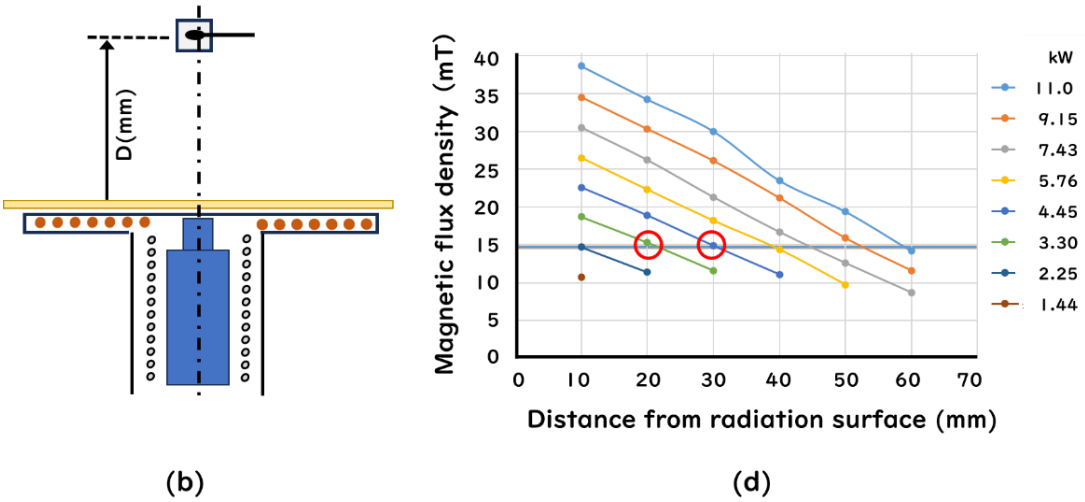

Figure 6. Density distribution profile of HTS-5010H and Hi-Heater 5010 radiator (**a**) Test scheme of HTS-5010H radiator; (**b**) Test scheme of Hi-Heater 5010 radiator; (**c**) Density distribution profile of HTS-5010H radiator; (**d**) Density distribution profile of Hi-Heater 5010 radiator. Red circles showed the radiation conditions of rat tumor treatment conducted under no clearance condition [13,14].

4. Effective 100kHz magnetic-flux-density at tumor locus in the standard treatment

In 2020, we have reported utility of heat-dose index and showed complete tumor regression in two rat tumor models using Hi-Heater 5010 radiator [13,14]. However, at that time, calibration of 100kHz magnetic flux density was not fully refined, and radiation intensity at tumor locus was specified with heat generation activity of MCL particle, namely around 750 J/g-MCL min [13,14].

As reported, MAT-LyLu rat tumor was treated at D=20mm and 3.30kW [13] and DMBA induced rat mammary tumor was treated at D=30mm and 4.45kW [14]. Here, retrospectively, effective density at tumor locus in the standard treatment condition was shown around 15mT (**Figure 6d**, red circle).

5. Clinical safety of 100kHz magnetic flux density in human body

During 2007~2011, clinical research had been conducted using HTS-5010H radiator [11], [12] p.1721. Treatment condition was controlled with tumor temperature index, but data were recorded in details. We tried to pick up safety-related data independent on heat-generating nanoparticles and analyze density distribution in patient bodies and discuss its causal relationship to adverse events.

5.1. Radiation condition and medical outcomes on safety

Cancer types of 7 patients and total 10 radiation sites were shown (**Table 1**, **Figure 7**). Radiation time has been fixed to standard 30min as animal models [13,14]. Cooling sheet and other devices was not applied to all patients, and local anesthesia was applied to a few patients. Radiation condition of output power (kW) and clearance C (mm) was picked up and shown with data of temperature monitoring on radiated skin surface (**Table 1**).

Medical findings on safety were summarized in **Table 1**. Adverse events on skin surface such as skin burn were not observed in all patients. Significant temperature rise on skin surface was not observed. All patients did not tell heat feeling, pain and discomfort during radiation even under no anesthesia condition. After radiation completion, slight tingling sensation was told by a patient #3, but was far from radiation

suspension. Change of vital signs was not observed in tested patient, and the last 3 patients were not hospitalized and permitted to bathe at home.

5.2. Magnetic flux density distribution in each patient body

Since relative magnetic permeability in human body was regarded as that in air, density distribution in patient body was deduced from density profile of HTS-5010H (**Figure 6c**) and radiation condition of each patient (**Table 1**). The formula of density distribution was converted with clearance C to; $y = 28.6\ e^{-0.044\ (x+C)}$ at 4.9kW and $y = 35.8\ e^{-0.045\ (x+C)}$ at 8.8k. And, terms of x and c were substituted with values of 10, 20 or 30 (mm) and each patient C value (mm) respectively, and densities at 10, 20 or 30mm locus from skin surface was shown at output power 4.9kW and 8.8kW respectively. Then, each-patient densities at 10, 20 or 30mm locus at each patient output power (kW) were shown by interpolation between the densities at 4.9kW and 8.8kW. Resulted density in patient body (y axis) was shown versus distance from skin surface (x axis) (**Figure 8**).

Magnetic flux density at skin surfaces were shown to range 19.0~34.9mT (**Figure 8**). Slight variation of skin temperature monitoring was shown not correlate to skin surface density. Then, density observed at skin surface was considered not causative to skin temperature rise and skin burn. Additionally, density distribution in human body shown at groin, breast, chin, chest and arm (**Figure 7, 8**) were considered not causative to vital change and quality of life declining. These data will be utilized as benchmark to test further tolerability under intensified radiation condition.

Table 1. Target cancers, radiation conditions and medical findings

Pts #	Cancer	Irradiation site	Anesthesia		Output (kW)	Clearance to skin (mm)	Density at skin (mT)	Skin temperature initial/end	Medical findings	
									Interview	Diagnosis
1	melanoma III 65 male	Right groin	one	local	const 0.9	0	19.9	34.8 / 35.0	No ache and heat feeling during and after treatment	No burn
2	melanoma (meta) IV 65 female	left side breast	A	local	avg 4.8	1 mm	27.3	36.1 / 37.1	No ache and heat feeling during and after treatment	No burn No abnormality of blood pressure and heart rate
			B				27.3	NT		
3	melanoma (meta) IIIc 38 female	left inner thigh	A	none	const 7.4	1 mm	34.9	36.0 / 37.3	No ache and heat feeling during and after treatment Slight tingling sensation during irradiation	No burn No abnormality of blood pressure and heart rate
			B				34.9	NT		
			C				34.9	NT		
4	papillary throid IV (meta) 80 female	neck under chin	one	local	const 6.8	13 mm	19	34.0 / 35.5	No ache and heat feeling during and after treatment	No burn, No abnormality Permittance of bathing
5	brest (meta) 80 female	right side chest	one	none	avg 3.5	5 mm	20.4	35.3 / 37.0	same as above	same as above
6	papillary throid (meta) 45 female	right front arm	one	local	const 7.2	3 mm	32.1	NT	same as above	same as above
7	tongue cancer (meta)	chest under chin	one	local	const 8.4	10 mm	23.2	NT	same as above	same as above

Patient #2 and #3 were radiated multiple sites separately (**Figure 7**). Clearance was defined from radiation surface to skin surface (**Figure 1d**). Magnetic flux density on skin surface was derived from density analysis in human body (**Figure 8**). Temperature of radiated skin surface was monitored with optical temperature probe attached on. Abbreviations: const; constant, avg; average, NT; not tested.

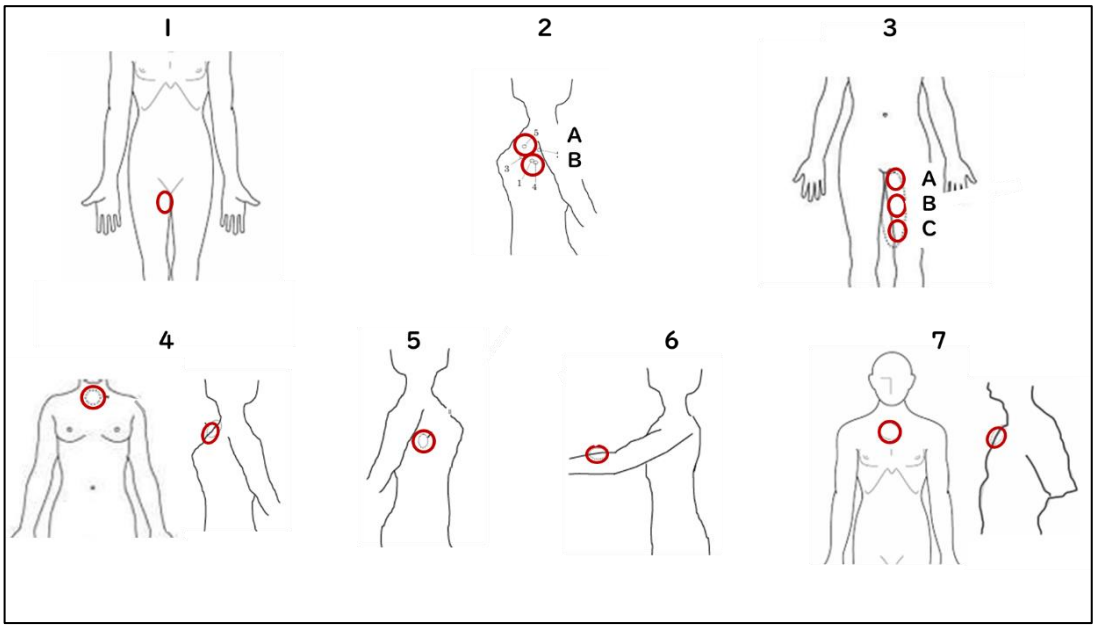

Figure 7. Body sites radiated with HTS-5010H radiator, red circles showed body sites of each patient radiated with 7cm Φ coil of HTS-5010H radiator.

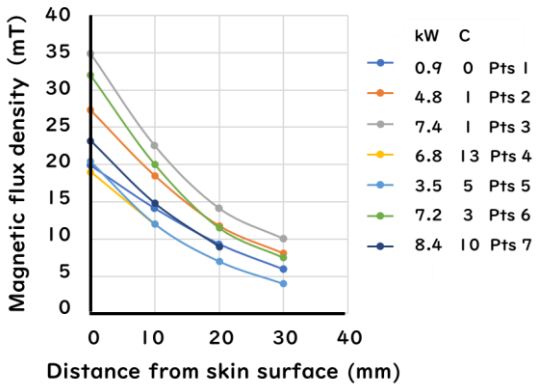

Figure 8. Density distribution in patient body shown from skin surface to inner body, each patient (Pts) was radiated at each body site (**Figure 7**) under annotated output power (kW) and clearance C (mm).

6. Clinical availability of the radiators and target cancers

HTS-5010H radiator was shown to achieve effective tumor density 15mT at D=20mm and 8.8kW (**Figure 6c**). Density distribution profile of this radiation condition was comparable to that of patient #3 (**Figure 8**), and HTS-5010H radiator could be safely applied to skin closed tumor located less than D=20mm. According to imaging data of laid human body [16], cancers such as melanoma, other skin cancers, breast, thyroid, rectal, head and neck cancers and subcutaneous metastasized cancers etc. would be involved in candidates for application.

Hi-Heater 5010 radiator was shown to achieve effective tumor density 15mT at D=52mm at 9.15kW (**Figure 6d**). Density distribution profile showed potential to treat distal tumor located around D=50~60mm at high output power 9.0~11kW. Skin surface density was interpolated almost-comparable to that of patient #3 (**Figure 8**), but safety of density distribution in human body remained unclear. According to imaging data of laid human body [16], cancers such as brain, pancreas, kidney, prostate, colon, stomach cancers etc. would be involved in potential candidates for application.

On the other hand, MFH®300F radiator at 100kH which formed cylindrical flat density zone between two 20cm Φ coils had been applied to brain cancer treatment, and tolerability for continuous 60min radiation was reported with magnetic field strength 10~14kA/m (corresponding to magnetic flux density 12.6~17.6mT) [10]. With all respect, we considered this epochal radiator would be available for nano-thermal ablation therapy in which tumors were treated at 15mT for continuous 30 min without temperature-probe canulation [1,13,14]. If possible, deep-seated tumors such as liver and lung cancers etc. would be involved in potential candidate of the therapy.

7. Eddy current mitigation and cancer-oriented radiator designing

Johanssen M. et al. reported tolerability of MFH®300F radiator was decreased in a use of prostate cancer treatment [9,17]. Tolerability of 10~14kA/m (12.6~17.6mT) was lowered to 4~5kA/m (corresponding to 5.0~6.3mT) due to pain and discomfort at perineum. Since this problem was only observed during radiation to high cross section, like pelvis, so-called boundary effect of Eddy current was pointed out. Namely, Eddy current generated from normal tissue (**Formula 2**) was disordered at boundary between low-conductive bone tissue and caused irregular current increase at skin hot spots [17] p.794. Theory of this boundary effect has been established and utilized in modern biomedical electromagnetics [18,19] for MRI (magnetic resonance imaging) technology and TMS (transcranial magnetic stimulation) therapy.

On the other hand, we showed clinical tolerability for much higher density at most using HTS 5010H radiator (**Figure 8**). This discrepancy would be explained by difference of density distribution profile of the radiator. Primarily, a small 7cm Φ coil (**Figure 1c**) would reduce total Eddy current generation from normal tissue due to less radius of induced current loop (**Formula 2**). Secondary, steep density declining (**Figure 6c**) would reduce risk of boundary effect due to less bone structure in subcutaneous tissue radiated.

This consideration indicated the subject of radiator matching to target cancer. Density distribution profile of HTS-5010H radiator (**Figure 6c**) would match to treatment of very skin-closed cancers better than others. Regardless answer, it would be worth noting that prostate cancers located at distance D=50~60mm from perinium or hypogastrium could be treated at 15mT by Hi-Heater 5010 radiator with less Eddy current from normal tissue and avoidance of pelvic bone radiation. These considerations indicated the subject of cancer-oriented radiator designing based on magnetic flux density.

8. Closing remarks on 100kHz radiator development

Development of clinical radiator for nano-thermal ablation therapy was started in 2004. According to “design input” in section **3**, two types radiators were constructed and characterized. To our experience, calibration of 100kHz magnetic flux density was laborious but definitely important. As exemplified trial products (**Figure 2b**), actual density measurement was only reliable in development phase. Frankly, outsourcing FEM density simulation of hat-shaped coil with protrusive ferrite core (**Figure 2c**) did mislead our development.

Sections from **3** to **6** were regarded as “design process” in Design Control Guidance [3] p.3. Here, we could draft “design output” as; “1) electromagnetic field frequency was set up at 100kHz to mitigate induction heating of normal tissue. 2) Output power of

radiator was made variable to control density of tumor locus and normal tissues. 3) To mitigate unnecessary exposure to normal tissue, radiation coil was set up at small size of 7cm Φ coil, and ferrite core was inserted to make sharp density distribution toward target tumor".

This seminar described significance of 100kHz magnetic flux density in clinical application of the nano-thermal ablation therapy. Universal measure of magnetic flux density is expected to clarify the concept of therapy and enable to discuss radiator designing, treatment control and target cancer matching etc. globally. Medical device development needed long-term efforts, that was represented with symbolic word of "design history file" in the Guidance [3] p.43. Author wishes this seminar will be helpful to describe the 1st page of design history file of 100kHz radiator used for novel solid cancer treatment modality [1,4] and accelerate its clinical application.

Acknowledgement

The authors would like to express sincere thanks Daivd West for consultation of administrative application, and Kohtaro Hirayama, Syuichiro Miyata for radiator construction.

Conflicts of Interests

The author declared no potential conflict of interest.

Appendix A

Commercial gauss-meter specific for 100kHz was noticed during manuscript preparation, although its availability was not tested (2D HF Magnetic field probe, AMF life systems MI USA).

Standard radiation condition of nano-thermal ablation therapy could take patients-friendly intervals during 30min radiation if needed, since treatment was controlled with total heat dose accumulated, independently on tumor temperature rise.

References

[1] Morino, T., Kawai, N., Ito, A., Kobayashi, T., & Yasui, T.: Novel nano-thermal ablation therapy using functionalized heat generating nanoparticles for solid cancer treatment. *World J Cancer & Oncology Research* **2023**, 2(1), 29-46. DOI: 10.31586/wjcor.2023.592

[2] Gneveckow U., Jordan A., Scholz R., Bruss V., Waldofner N., Ricke J., Feussner A., Hildebrandt B., Rau B., Wust P. Description and characterization of the novel hyperthermia-and thermoablation-system MFH300F for clinical magnetic fluid hyperthermia. *Med Phys* **2004**, 31: 1444-1451. DOI: 10.1118/1.1748629

[3] Design Control Guidance for Medical Device Manufacturer. **1997**, www.fda.gov/media/116573/download

[4] Gilchrist R., Medal R., Shorey W., Hanselman R., Parrott J., Taylor B. Selective inductive heating of lymph nodes. *Ann Surg* **1957**, 141: 596-606. DOI: 10.1097/00000658-195710000-00007

[5] Gilchrist R., Shorey W., Hanselman R., DePeyster F., Yang J., Medal R. Effects of electromagnetic heating on in viscera: A preliminary to the treatment of human tumors. *Ann Surg* **1965**, 161: 890-896. DOI: 10.1097/00000658-196506000-00008

[6] Gordon R. T., Hines J., Gordon D. Intracellular hyperthermia, A biophysical approach to cancer treatment via intracellular temperature and biophysical alteration. *Med Hypothesis* **1979**, 5: 83-102. DOI: 10.1016/0306-9877(79)90063-x

[7] Jordan A., Wust P., Fahling H., John W., Hinz A., Felix R. Inductive heating of ferromagnetic particles and magnetic fluids: physical evaluation and their potential for hyperthermia. *Int J Hyperthermia* **1993**, 9: 51-68. DOI: 10.3109/02656739309061478

[8] Yanase M., Shinkai M., Honda H., Wakabayashi T., Yoshida J., Kobayashi T. Intracellular hyperthermia for cancer using magnetite cationic liposomes: An *in vivo* study. *Jpn J of Cancer Res* **1998**, 89: 463-469. DOI: 10.1111/j.1349-7006.1998.tb00586.x

[9] Johannsen M., Gneveckow U., Eckelt L., Feussner A., WaldÖFner N., Scholz R., Deger S., Wust P., Loening S., Jordan A. Clinical hyperthermia of prostate cancer using magnetic nanoparticles: Presentation of a new interstitial technique. *Int J Hyperthermia* **2005**, 21: 637-647. DOI: 10.1080/02656730500158360

[10] Maier-Hauff K., Rothe R., Scholz R., Gneveckow U., Wust P., Thiesen B., Feussner A., Von Deimling A., Waldo¨fner N., Felix R., Jordan A. Intracranial thermotherapy using magnetic nanoparticles combined with external beam radiotherapy: Results of a feasibility study on patients with glioblastoma multiforme. *J Neurooncol* **2007**, 81: 53–60. DOI.org/10.1007/s11060-006-9195-0

[11] Matsumoto K., Kobayashi T., Saida T.. Magnetic Hyperthermia. *Nippon Rinsyo*, **2013**, 71. Suppl 4.

[12] Kobayashi T., Kakimi K., Nakayama E., Jombow K. Antitumor immunity by magnetic nanoparticle-mediated hyperthermia. *Nanomedicine* **2014**, 9: 1715-1726. DOI: 10.2217/nnm.14.106

[13] Morino T., Tanoue S., Miyata S., Hirayama K., Ito A., Etani T., Naiki T., Kawai N., Yasui T. Heat dose index *in vivo* for cancer herapy using heat-generating nanoparticles named magnetite cationic liposomes and alternating magnetic field radiator. *Thermal Med* **2020**, 36: 47-58. DOI: 10.3191/thermalmed.36.47

[14] Morino T., Ito A., Etani T., Naiki T., Kawai N., Yasui T. Heat dose based large tumor treatment with multiple site injections of heat-generating nanoparticles dispersible within tumor tissue. *Thermal Med* **2020**, 36: 91-98. DOI: 10.3191/thermalmed.36.101

[15] Motoyama J., Hakata T., Kato R., Yamashita N., Morino T., Kobayashi T., Honda H. Size dependent heat generation of magnetite nanoparticles under AC magnetic field for cancer therapy. *BioMag Res Tech* **2008**, 6: e4. DOI: 10.1186/1477-044X-6-4

[16] Moran C.M., Thomson A.J.W., Preclinical ultrasound imaging - A review of techniques and imaging applications. *Front. Phys* **2020**, 8: 124. DOI: 10.3389/fphy.2020.00124

[17] Johannsen M, Thiesen B, Wust P, et al. Magnetic nanoparticle hyperthermia for prostate cancer. *Int J Hyperthermia* **2010**, 26(8): 790-795. DOI: 10.3109/02656731003745740

[18] Thomas W. B., Soma V., Peter B., Andreas S., Philippe B. Characterization of the electrical conductivity of bone and its correlation to osseous structure. *Scientific report* **2018**, 8: 8601. DOI:10.1038/s41598-018-26836-0

[19] Syrek, P.; Skowron, M.; Kapustka, P. Eddy current distribution in magnetotherapy of bones: A qualitative and quantitative study. *Appl Sci* **2025**, 15; 9892. https://DOI.org/10.3390/ app15189892.